Rapid visualization of nonmelanoma skin cancer

Ethan Walker, MD, PhD,[a] Margaret Mann, MD,[h] Kord Honda, MD,[h] Allison Vidimos, MD,[i] Mark D. Schluchter, PhD,[b] Brian Straight, PhD,[e] Matthew Bogyo, PhD,[f,g] Daniel Popkin, MD, PhD,[h] and James P. Basilion, PhD[a,c,d]

Cleveland, Ohio, and Stanford, California

Background: Mohs micrographic surgery examines all margins of the resected sample and has a 99% cure rate. However, many nonmelanoma skin cancers (NMSCs) are not readily amenable to Mohs micrographic surgery. This defines an unmet clinical need to assess the completeness of non-Mohs micrographic surgery resections during surgery to prevent re-excision/recurrence.

Objective: We sought to examine the utility of quenched activity-based probe imaging to discriminate cancerous versus normal-appearing skin tissue.

Methods: The quenched activity-based probe GB119 was applied to NMSC excised from 68 patients. We validated activation of the probe for hematoxylin-eosin–confirmed cancerous tissue versus normal-appearing skin tissue.

Results: Topical application of the probe differentiated basal cell carcinoma and squamous cell carcinoma from normal-appearing skin with overall estimated sensitivity and specificity of 0.989 (95% confidence interval 0.940-1.00) and 0.894 (95% confidence interval 0.769-0.965), respectively. Probe activation accurately defined peripheral margins of NMSC as compared with conventional hematoxylin-eosin–based pathology.

Limitations: This study only examined NMSC debulking excision specimens. The sensitivity and specificity for this approach using final NMSC excision margins will be clinically important.

Conclusions: These findings merit further studies to determine whether quenched activity-based probe technology may enable cost-effective increased cure rates for patients with NMSC by reducing re-excision and recurrence rates with a rapid and easily interpretable technological advance. (J Am Acad Dermatol 2017;76:209-16.)

Key words: cathepsin-B; cathepsin-L; molecular optical imaging; nonmelanoma skin cancer; quenched activity-based probe; re-excision rate; topical application.

From the Departments of Biomedical Engineering,[a] Epidemiology and Biostatistics,[b] and Radiology,[c] and National Foundation for Cancer Research Center for Molecular Imaging,[d] Case Western Reserve University, Cleveland; Akrotome Imaging Inc, Cleveland[e]; Departments of Pathology[f] and Microbiology and Immunology,[g] Stanford University; Department of Dermatology, University Hospital, Cleveland[h]; and Department of Dermatology, Cleveland Clinic Foundation.[i]

This study was supported by an R21 (5R21CA183160-02) and P30 AR039750 award (Dr Basilion) and a subcontract to Dr Basilion from 5R21CA183160-02 awarded to Dr Straight of Akrotome Imaging Inc. The funding sources had no role in the design and conduct of the study; collection, management, analysis, and interpretation of the data; preparation, review, or approval of the manuscript; or decision to submit the manuscript for publication.

Disclosure: Drs Basilion and Bogyo are both board members and co-founders of Akrotome Imaging Inc. Dr Straight is the chief executive officer of Akrotome Imaging Inc. Drs Walker, Mann, Honda, Vidimos, Schluchter, and Popkin have no conflicts of interest to declare.

The abstract of this study was presented orally at the World Molecular Imaging Congress; Honolulu, Hawaii; September 2-5, 2015.

eFigures and eTable are available at http://www.jaad.org.

Accepted for publication September 2, 2016.

Reprint requests: James P. Basilion, PhD, Departments of Biomedical Engineering, Radiology, and Pathology Case Center for Imaging Research, Case Western Reserve University, Wearn Bldg, Room B42, 11100 Euclid Ave, Cleveland, OH 44106-5056. E-mail: james.basilion@case.edu.

Published online November 19, 2016.

0190-9622/$36.00

http://dx.doi.org/10.1016/j.jaad.2016.09.008

Nonmelanoma skin cancer (NMSC) is the most common form of human cancer with approximately 3.5 million cases diagnosed in the United States in 2006 and approximately 4 million diagnosed each year hence.[1,2] Approximately 80% of all NMSC are basal cell carcinomas (BCC) with most of the remaining being squamous cell carcinomas (SCC).[3] Several approaches to ensure complete removal of diseased tissue with minimal resection of normal tissue have been developed, including Mohs micrographic surgery (MMS)[4,5] that checks margins during surgery and has the highest cure rate of all approaches (99%). However, conventional or non-MMS resection is the most common surgical approach for skin cancers representing approximately 75% of surgical procedures for BCC and SCC[1] and has much lower cure rates than MMS. Well-differentiated SCC cure rates approach 81% using non-MMS procedures but decreases to 46% for poorly differentiated lesions.[6] Resections of BCC fare slightly better with approximately 93% cure rates.[7] Because rates are related to the size of margins that the dermatologist removes, conventional resections generally result in larger resections of normal tissue to ensure clear margins, which are determined by conventional pathology several days after the surgery.[8,9] Here we describe an easily interpretable methodology that could be cost-effectively deployed and rapidly executed to enable surgeons to better assess peripheral surgical margins, thus reducing the amount of normal tissue resected during conventional NMSC excisions.

The study presented exploits molecular imaging technology[10,11] to target overexpressed skin cancer-associated cathepsin proteases.[12-16] The technique uses a cysteine cathepsin selective class of near-infrared fluorescent quenched activity-based probes (QABPs)[17] effective for imaging tumor-expressed cathepsins, in vitro and in vivo,[18-22] which are hydrophobic and readily penetrate the skin. Interaction of QABPs with target proteases results in de-quenching and production of a fluorescent signal. Here, GB119 is used to target cancer cysteine cathepsin enzymes to discriminate NMSC from normal-appearing skin ex vivo creating a 2-dimensional (2D) fluorescent map for each sample. Specifically, ex vivo topical administration of this probe is used to develop a standardized method to differentiate cancer from normal-appearing skin in excised human skin cancer specimens.

CAPSULE SUMMARY

- Quenched activity-based probes have been used to localize brain cancer.
- Rapid fluorescent quenched activity-based probe visualization technique highlights areas positive for hematoxylin-eosin–defined nonmelanoma skin cancer with great accuracy.
- Quenched activity-based probes may rapidly and easily identify residual nonmelanoma skin cancers during excision.

METHODS

Collection of human skin specimens

This study was approved by the University Hospitals Case Medical Center Institutional Review Board (protocol #12-05-17). Discarded skin tissues containing previously diagnosed BCC or SCC were taken during debulking for MMS (eTable I) for this prospective case series. All BCC/SCC debulk specimens greater than or equal to 1 × 1 cm were processed, imaged, and analyzed.

Ex vivo imaging of human skin specimens

Freshly removed debulk specimens were covered with saline-soaked gauze and delivered to the laboratory 90 to 120 minutes after surgery. Samples were rinsed with saline, blotted dry with gauze, followed by baseline imaging (0 minutes). Probe GB119 (10 μmol/L in dimethyl sulfoxide) (Sigma-Aldrich, St Louis, MO) was applied to the dermal side. After 5 minutes, excess probe was rinsed from the sample with saline and the dried sample was imaged in the Maestro imaging system (PerkinElmer, Waltham, MA) with a near-infrared filter set. Two sectioning approaches were used (Graphical abstract, Step 4). In the breadloaf section, ink was used to mark the location of fluorescence before signals sectioning.

Analysis of Cy5-fluorescence

Fluorescence was measured and pseudo-color images were derived using Maestro and supplied software 3.0.1.2 (PerkinElmer). Levels of autofluorescence (0 minutes) were subtracted from fluorescence at 5 minutes with GB119 and remaining signal intensity was pseudo-colored. Signal was mapped onto the surface of the samples and inked in some cases. Samples were immersed in optimal cutting temperature compound, snap-frozen, and kept at −80°C for further study.

Histologic and immunofluorescent analysis of human skin samples

Frozen blocks were sectioned (10 μm) in a breadloaf manner at −30°C (Leica-CM3050S).

Abbreviations used:

BCC: basal cell carcinoma
H&E: hematoxylin-eosin
IHC: immunohistochemistry
MMS: Mohs micrographic surgery
NMSC: nonmelanoma skin cancer
QABP: quenched activity-based probe
SCC: squamous cell carcinoma
2D: 2-dimensional

The cryosections were then fixed and stained with hematoxylin-eosin (H&E). For en face sectioning specimens were not inked and the entire frozen blocks were sectioned from dermal side toward epidermal side. Immunohistochemistry (IHC) for activated GB119 and cathepsin expression was performed on adjacent 10-μm sections for detection of unquenched/activated GB119 and cathepsin−L or −B, as described in Walker et al.[11] Tissue nuclei were contrasted with Fluoro-Gel-II with 4′,6-diamidino-2-phenylindole (Electron Microscopy Sciences, Hatfield, PA).

Microscopy

Fluorescent images were viewed with a Leica-DM4000B microscope (bandpass = 480/527, anticathepsin-L and -B and bandpass = 560/645, anti-Cy5) and analyzed with QCapturePro-7 software (Leica Microsystems, Buffalo Grove, IL). An Olympus-VS120/S5 (Olympus Life Science, Tokyo, Japan) versatile microscope-based scanner was used to generate histologic images larger than a single field of view. Overlays between H&E and Cy5-fluorescent images were done manually. Technically validated results were included in the analyses and no data were excluded as outliers. H&E examination of BCC/SCC slides was performed by 2 pathologists without knowledge of Cy5-fluorescent imaging or other information. All annotations of the position of BCC/SCC and normal tissue were made by pathologists directly on the histologic slides via marking pens.

Sensitivity and specificity analysis

Sensitivity and specificity were estimated as binomial proportions and exact 95% confidence intervals were calculated. The data set consisted of 55 samples from 54 patients (35 BCC and 20 SCC). A total of 72 histology sections (slides), containing 137 regions of interest were examined. Ninety regions of interest having tumor and 47 marked as having no tumor were treated as independent observations in a per-spot analysis; these sample sizes allowed estimation of overall sensitivity and specificity within ± 0.06 and 0.09, respectively, using 95% confidence intervals when true sensitivity or specificity equaled 0.90. The subtypes of all available samples are reported in eTable I.

RESULTS

QABP fluorescence discriminates between NMSC and normal tissue ex vivo

First we determined that normal-appearing human skin does not activate our imaging probe, GB119, after topical application (Fig 1, *A*). After topical application of GB119 to the nonepidermal surface of a sample containing either BCC or SCC there was significant probe activation resulting in increased fluorescence viewed en face (Fig 1, *B* and *C*). Pathological correlation of the location of cancer and fluorescent signal in conventional breadloaf sections taken from these specimens showed a good association and clear demarcation between normal and cancerous tissues (lower panels Fig 1, *B* and *C*).

The sensitivity and specificity of the probe for detecting NMSC in BCC samples were 100% and 87%, respectively (Table I). Similarly, using SCC samples only, the sensitivity and specificity were 97% and 92%, respectively (Table I). There were no significant differences in probe activation among the subtypes of BCC and SCC and signal strength was significantly higher in NMSC versus normal-appearing skin (eFig 1 and eTable I).

Presence of activated GB119 correlates with the expression of cathepsin-L in and around skin cancer

To further validate and characterize the relationship of probe activation with its cognate enzyme, IHC analysis was performed for cathepsin proteases (Fig 2). Breadloaf sections were prepared from normal-appearing, BCC, and SCC skin samples that were treated with GB119, and then underwent H&E staining and IHC for cathepsins and the activated probe. The results confirm that normal tissue expresses low levels of cathepsins and shows little to no activation of the probe. Within cancer lesions, cathepsin expression was elevated and correlated to probe activation, with the highest probe signal and expression of cathepsins occurring at the edge of the cancer nests both in BCC and SCC (Fig 2). Controls confirmed the specificity of the assay (eFig 2 in the Supplement). These studies also demonstrated that probe activation occurred in the thickest sample analyzed, approximately 2.5 mm (eFig 3 and eTable I).

Fluorescence imaging defines the cancer diameter at different depths within the skin cancer lesion

Next, 2D epifluorescence imaging of flat skin samples was correlated to the location of cancer

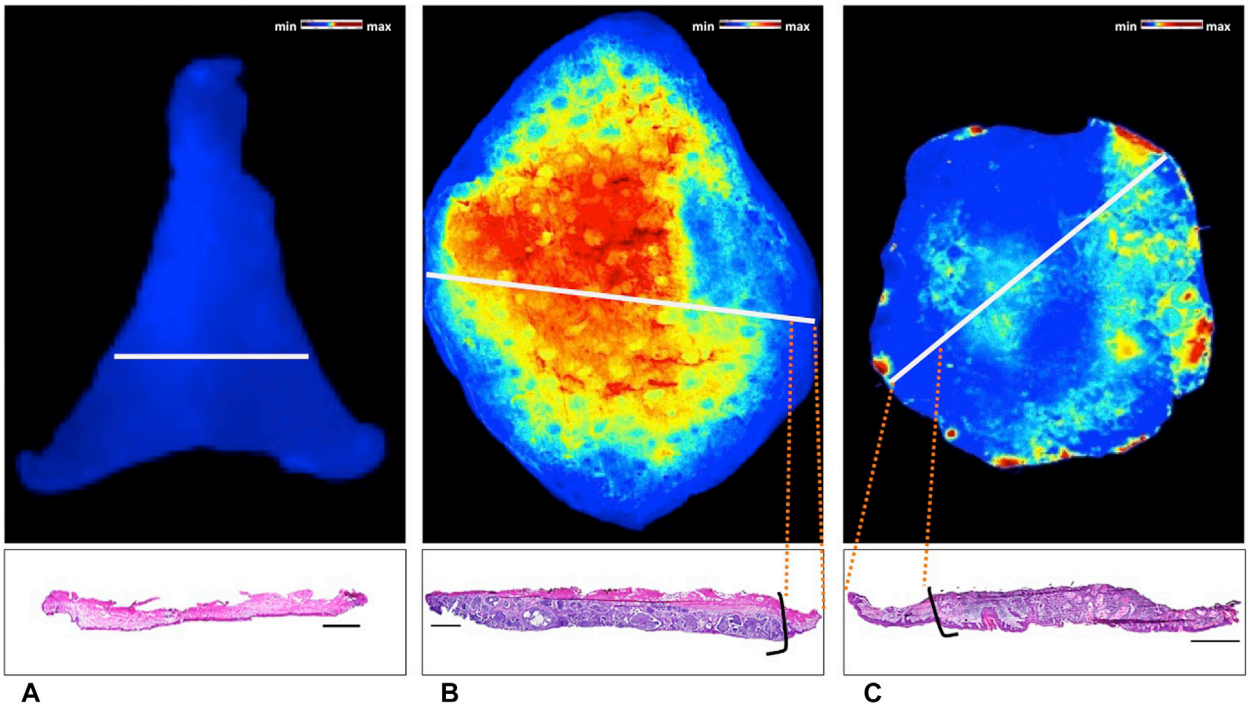

Fig 1. Breadloafed skin cancers: probe activation corresponds to the presence of cancer. Activation of GB119 and corresponding pathology from breadloaf sections of specimens. **A**, Normal tissue. **B**, Basal cell carcinoma. **C**, Squamous cell carcinoma. Presence of pathology ink on the dermal side of the samples used to mark the areas of high Cy5-fluorescence. *White lines*, plane of section. *Black lines*, cancer zone borders. Scale bars = 2 mm.

Table I. Analysis of relationship between GB119 activation and presence of skin cancer in human skin samples

Measure	Group examined	Regions of interest	Sensitivity/specificity (positives/total specimens)	95% Confidence interval (2-sided)
Sensitivity	All patients	90	0.989 (89/90)	0.940-1.000
	BCC only	56	1.000 (56/56)	0.936-1.000
	SCC only	34	0.971 (33/34)	0.847-1.000
Specificity	All patients	47	0.894 (42/47)	0.769-0.965
	BCC only	23	0.870 (20/23)	0.664-0.972
	SCC only	24	0.917 (22/24)	0.730-0.990

For these studies 55 patient samples were assessed: 35 BCC (nodular = 8, micronodular = 10, infiltrative = 4, superficial = 8, mixed pathology = 5) and 20 SCC (well differentiated = 15, mildly differentiated = 3, poorly differentiated = 0, mixed pathology = 2).
Sensitivity is (true positives/ (true positives + false negatives); Specificity is (true negatives/ (false positives + true negatives).
BCC, Basal cell carcinoma; *SCC*, squamous cell carcinoma.

within different depths of the skin specimens. Fig 3 shows a BCC skin sample topically treated with GB119, imaged (Fig 3, *A*), frozen, and en face sectioned followed by histology and IHC to identify the location of activated probe and NMSC. Sections from 4 different depths from the dermal site of application were assessed by blinded pathologists (up to 0.8 mm [Fig 3, *B*] and up to 2.5 mm [eFig 3]) and bolded contour lines representing the cancer (black/purple) and inflammation (red) perimeters at each depth were superimposed on the 2D fluorescence image of the corresponding skin sample (Fig 3, *C*), the larger distances representing the farthest distance from the dermal site of probe application.

These data show the heterogeneous location of the edge of cancerous tissue at different depths within the tissue specimens. The inflammatory milieu of cancer was found both inside and at the edge of the cancer lesions at different depths. As is evident in both Fig 3, *B* and *C*, the combination of the histology contour maps depicting cancer and its inflammatory milieu completely outline the fluorescence maps, demonstrating that the fluorescence signal, which comes from different depths within the lesion, accurately marks the perimeter of the

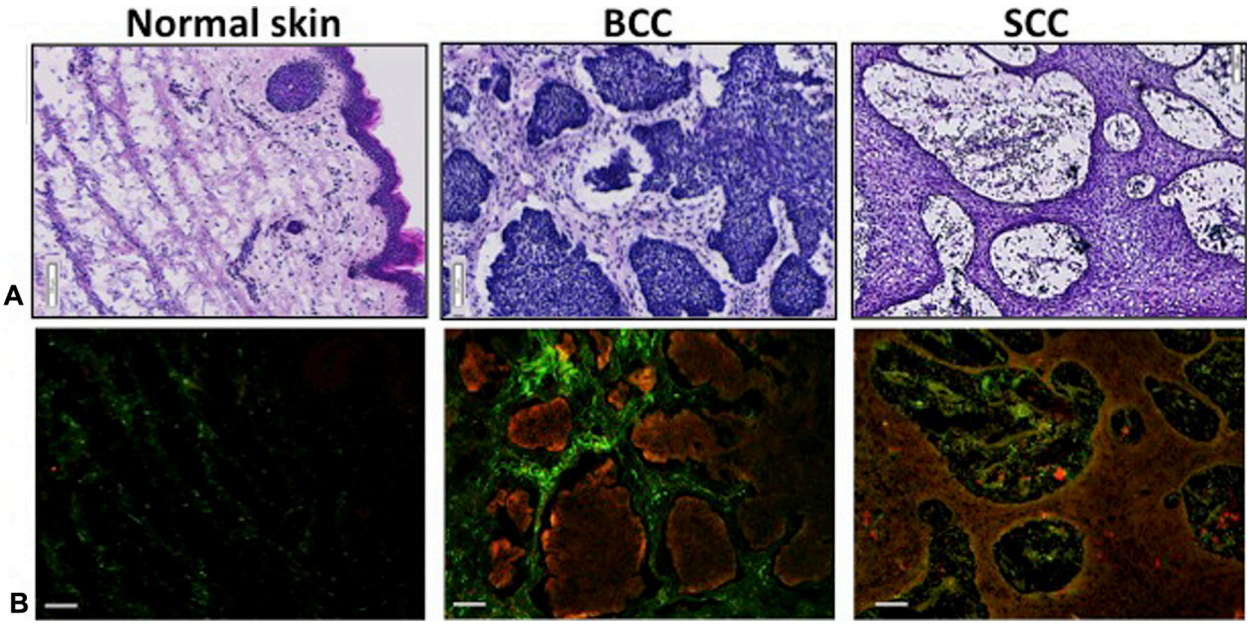

Fig 2. Basal cell carcinoma (*BCC*) and squamous cell carcinomas (*SCC*): correlation of probe activation to cancer and cathepsin (CTS)-L expression in samples. **A**, Hematoxylin-eosin histology of breadloaf sections of human skin samples pretreated with GB119. **B**, Immunohistochemistry of the breadloaf section shows colocalization of CTS-L (*green*) and Cy5 (activated probe [*red*]) in image overlays. Scale bars = 100 μm.

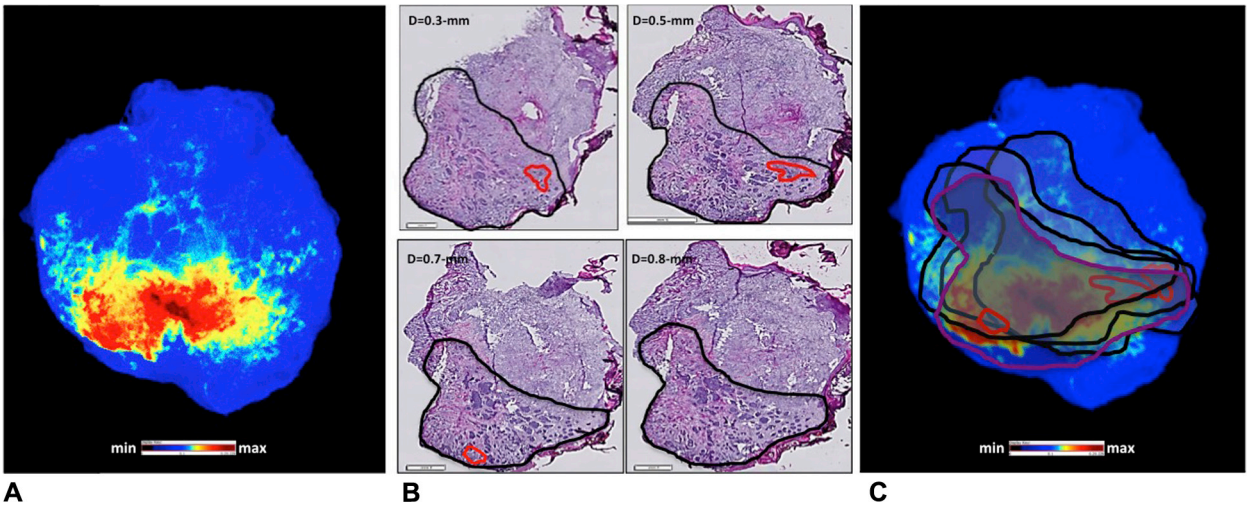

Fig 3. Basal cell carcinoma: correlation of pathology throughout the specimen with epifluorescence imaging. **A**, Cy5-fluorescent image of skin sample pretreated with GB119. **B**, En face section histology at different depth; *bold contour markings* = pathologist hematoxylin-eosin (H&E)-mapped cancer perimeter. **C**, Overlay of contour markings on the fluorescence image of the skin sample; *red contours* = tissue inflammation. Scale bars (H&E) = 1 mm and 2 mm (*large*).

cancerous lesion for BCC samples and potentially could be used to inform the location of peripheral margins for conventionally resected skin cancer. Similar results were obtained for SCC skin samples where sections at the depths up to 1.9 mm were analyzed by pathologists (eFig 4 and eTable I).

To determine the exact correlation of fluorescence signal within cancer borders, the data from Fig 3 were used to identify regions depicting normal tissue, regions of cancer only, and the interface between cancer and normal tissues (rectangles, Fig 4, *A*). These regions were then further analyzed

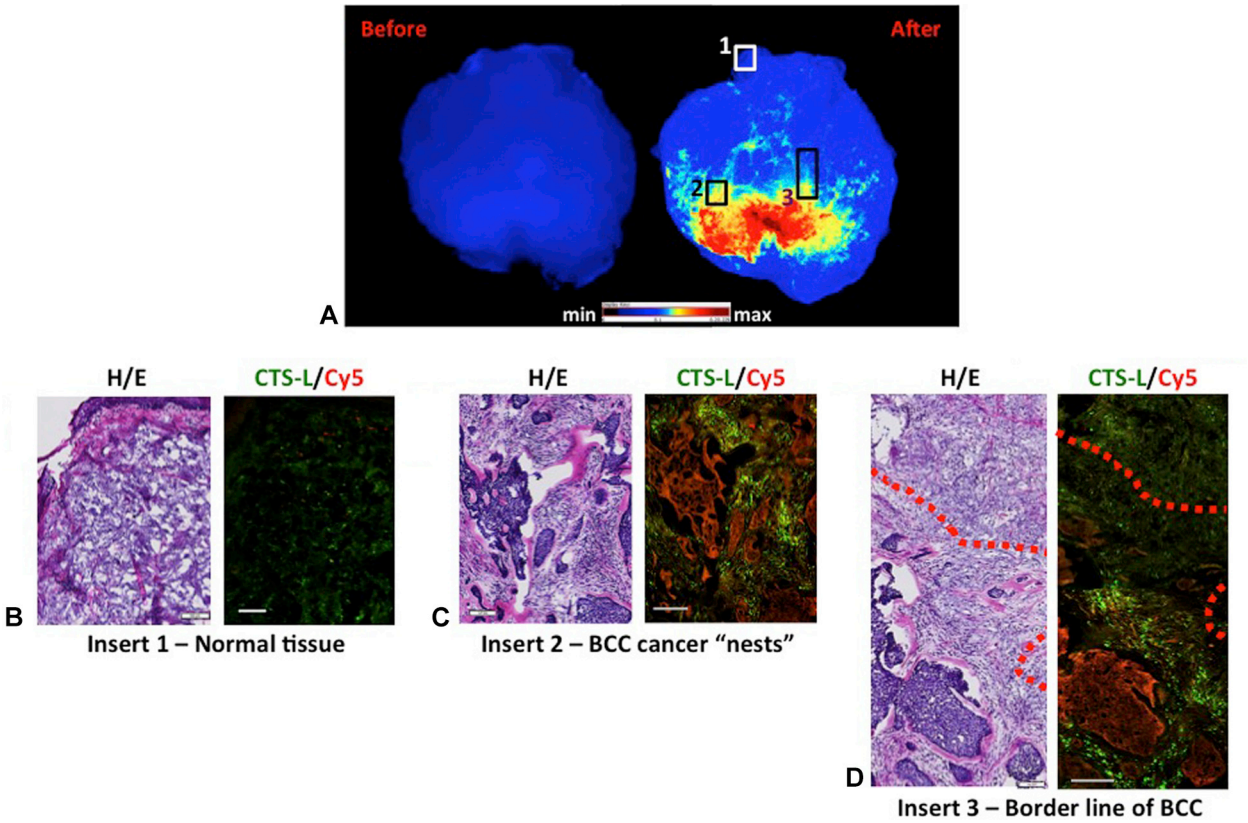

Fig 4. Basal cell carcinoma (*BCC*): microscopic analysis of regions representing different locations within the sections. **A**, Fluorescent images of BCC skin specimen treated with GB119. **B** to **D**, Overlay of cathepsin (*CTS*)-L (*green*) and Cy5 (*red*) from different locations of the sample. *Red dotted line* = borderline between BCC and normal tissue. Scale bars = 100 μm. *H&E*, Hematoxylin-eosin.

to achieve a more detailed correlation of the location of cancer, cathepsin-L, and activated GB119 probe. Fig 4, *B-D*, show that there was a high degree of correlation between the presence of fluorescence and the location of BCC lesions and normal-appearing skin. Similar results were obtained for SCC samples, and inflammation associated with the sample was also observed in the regions with the highest level of GB119 activation and demonstrated cathepsin B is also associated with probe activation (eFigs 4, 5, and 6). The effect of blood clots affecting signal was demonstrated in eFig 7.

DISCUSSION

The results of this study suggest a potentially promising approach to the surgical resection of NMSC, showing that the QABP GB119 topically applied to tissue after excision can discriminate between normal-appearing skin and either BCC or SCC tissues within minutes. Following the breadloafing procedure outlined in the graphical abstract, these studies used 55 skin cancer specimens to demonstrate 90% or higher overall sensitivity and specificity for detecting BCC/SCC cancer lesions in a background of normal human tissue (Table I and Fig 1). Further, subtypes of BCC (nodular, micronodular, superficial, and infiltrative) and SCC (well differentiated) were detected equally well by this technology (eFig 1 and eTable I). Using an IHC assay for detection of activated GB119,[11] it was possible to ascertain microscopic resolution of the location of activated probe, protease expression, and cancerous cells showing that they colocalized at almost all locations (Figs 2, 4, e3, e5, e6, and e8). Comparing probe activation and pathological findings using en face sections at different depths below the application surface revealed that the perimeter of the 2D fluorescence image reproducibly outlined the location of cancer at all depths assessed. Taken together, these data demonstrate that GB119/cathepsin-dependent fluorescent images of NMSC excisions discriminate cancerous tissue from normal-appearing skin defining the peripheral margins of BCC/SCC lesions and are not significantly affected by light scatter or diffusion by the tissue.

Although previous efforts to enhance the detection and removal of skin cancer have resulted in the development of several optical fluorescence techniques,[23-25] these approaches rely both on systemic and local administration of the imaging agents or imaging using endogenous differences in contrast. However, none of these methods have yet been clinically approved in the United States. For example, skin cancers investigators attempted to use autofluorescence of skin cancer lesions,[26] photodynamic diagnosis,[27,28] or the use of a near-infrared fluorescent-labeled skin cancer targeted antibody, panitumumab-IRDye800.[29] Each of these approaches, however, has drawbacks, resulting in lower sensitivity and specificity, longer times (6 hours) for lesion discrimination, or the need for systemic injection with the potential of immunogenic response. Further, the systemically administered agents require costly phase-I to -III clinical trials to move toward clinical use. This approach using topical application of imaging probes to detect cancer-associated enzymes[10,30] is the only example to show ex vivo topical application of imaging probes to excised samples can rapidly visualize tumor margins during surgical procedures. Our previous studies demonstrated the feasibility of this approach using a brain tumor model[10] and now we use this technology to demonstrate for the first time to our knowledge its potential to impact conventional skin cancer resections in human beings. We are currently conducting an institutional review board—approved trial to examine the specificity and sensitivity of this approach in the setting of such conventional wide local excisions. Ultimately, we envision this technology to inform the surgeon of margin status within 15 minutes of a conventional excision. This may enable surgeons to use minimal margins (eg, 3-mm vs up to 5-mm margins used for nonmorpheaform BCCs) while obtaining similar or possibly more favorable recurrence rates. Commercialization of such a product would need to be economically viable to enable community practitioners to adopt this technology. Finally, we envision that this technology could improve health care access for superior margin control for those ineligible for MMS for a variety of reasons; but QABP would not provide significant improvement as an additional step in modern MMS workflows.

In agreement with previous studies,[10,11,25,31] the data show close correlation between probe activation and the presence of cancer and areas of inflammation, which contain macrophages, activate GB119, and are presumably an important source of activated cathepsins. Areas of strong accumulation of macrophages (eFig 5, *B*, region 4) at the cancer lesion/normal tissue interface stained with both anticathepsin-L and for activated probe. Also GB119 activation occurs in the extracellular milieu of cancer cells, a likely result of the fact that cathepsins can be secreted from the cells. Because cathepsin-B (eFig 6) expression is also associated with GB119 activation, it seems likely that Cy5-fluorescence imaging depends not only on presence of cathepsin-L but rather represents GB119/multicathepsin-dependent fluorescence from the top to bottom of the skin samples. These studies demonstrate that overexpression of cathepsin proteases is prevalent in both BCC and SCC lesions, making cathepsins an excellent biomarker for skin cancer margin detection.

The study also addressed potential limitations to this approach. A particular concern is the effect of surgery, tissue thickness, and tissue structures on the ability to visualize probe fluorescence. The presence of activated probe was detected in SCC zones but not in the cancer cell-free zones at the depth ~1.9 mm (eFig 4, *B*, and eFig 5, *B*) and correlated to the deepest cancer in the specimens that were collected: 2.5 mm (eFig 3). These depths of detection are well suited to detect cancer in the peripheral margins of the cancer indicating low impact, if any, of scattering or absorption of near-infrared light for imaging quality. In this study, we observed no difference in detection signal for the 4 subtypes of BCC and 2 subtypes of SCC examined (eFig 1). It will be critical to determine if this pattern is observed for other subtypes of BCC and SCC and to ensure that benign fibrosis/scarring in the absence of cancerous cells in addition to benign growths, eg: do trichoepitheliomas produce a QABP signal similar to tumor?

Bleeding that might occur during sample preparation could cause another potential limitation to the technique (eFig 7). Depending on the location, clot attenuation may compromise the ability to assess surgical margins ex vivo. However, blood clots in these samples were likely a result of the transport time to the research laboratory: 90 to 120 minutes. Further development of imaging protocols will involve the use of only fresh-excised specimens imaged within 10 minutes of resection using a portable imaging device, making them virtually free from clots and addressing other practical limitations of the approach presented here.

REFERENCES

1. Connolly SM, Baker DR, Coldiron BM, et al, Ad Hoc Task Force. AAD/ACMS/ASDSA/ASMS 2012 appropriate use criteria for Mohs micrographic surgery: a report of the American Academy of Dermatology, American College of Mohs Surgery,

American Society for Dermatologic Surgery Association, and the American Society for Mohs Surgery. *J Am Acad Dermatol*. 2012;67(4):531-550.
2. Rogers HW, Weinstock MA, Harris AR, et al. Incidence estimate of nonmelanoma skin cancer in the United States, 2006. *Arch Dermatol*. 2010;146(3):283-287.
3. Rubin AI, Chen EH, Ratner D. Basal-cell carcinoma. *N Engl J Med*. 2005;353(21):2262-2269.
4. Mohs FE. Chemosurgical treatment of cancer of the skin; a microscopically controlled method of excision. *JAMA*. 1948; 138(8):564-569.
5. Mikhail GR, ed. *Mohs micrographic surgery*. Philadelphia (PA): W.B. Saunders; 1991.
6. Rowe DE, Carroll RJ, Day CL Jr. Prognostic factors for local recurrence, metastasis, and survival rates in squamous cell carcinoma of the skin, ear, and lip. Implications for treatment modality selection. *J Am Acad Dermatol*. 1992; 26(6):976-990.
7. Griffiths RW. Audit of histologically incompletely excised basal cell carcinomas: recommendations for management by re-excision. *Br J Plast Surg*. 1999;52(1):24-28.
8. Motley R, Kersey P, Lawrence C. Multiprofessional guidelines for the management of the patient with primary cutaneous squamous cell carcinoma. *Br J Dermatol*. 2002;146(1):18-25.
9. Thomas DJ, King AR, Peat BG. Excision margins for nonmelanotic skin cancer. *Plast Reconstruct Surg*. 2003;112(1):57-63.
10. Cutter JL, Cohen NT, Wang J, et al. Topical application of activity-based probes for visualization of brain tumor tissue. *PLoS One*. 2012;7(3):e33060.
11. Walker E, Gopalakrishnan R, Bogyo M, Basilion JP. Microscopic detection of quenched activity-based optical imaging probes using an antibody detection system: localizing protease activity. *Mol Imaging Biol*. 2014;16(5):608-618.
12. Jedeszko C, Sloane BF. Cysteine cathepsins in human cancer. *Biol Chem*. 2004;385(11):1017-1027.
13. Fröhlich E, Möhrle M, Klessen C. Cathepsins in basal cell carcinomas: activity, immunoreactivity and mRNA staining of cathepsins B, D, H and L. *Arch Dermatol Res*. 2004;295(10): 411-421.
14. Kawada A, Hara K, Kominami E, et al. Expression of cathepsin D and B in invasion and metastasis of squamous cell carcinoma. *Br J Dermatol*. 1997;137(3):361-366.
15. Kawada A, Hara K, Kominami E, Kobayashi T, Hiruma M, Ishibashi A. Cathepsin B and D expression in squamous cell carcinoma. *Br J Dermatol*. 1996;135(6):905-910.
16. Ishida M, Kojima F, Okabe H. Cathepsin K expression in basal cell carcinoma. *J Eur Acad Dermatol Venereol*. 2013;27(1):e128-130.
17. Baruch A, Jeffery DA, Bogyo M. Enzyme activity — it's all about image. *Trends Cell Biol*. 2004;14(1):29-35.
18. Blum G, Mullins SR, Keren K, et al. Dynamic imaging of protease activity with fluorescently quenched activity-based probes. *Nat Chem Biol*. 2005;1(4):203-209.
19. Blum G, von Degenfeld G, Merchant MJ, Blau HM, Bogyo M. Noninvasive optical imaging of cysteine protease activity using fluorescently quenched activity-based probes. *Nat Chem Biol*. 2007;3(10):668-677.
20. Sexton KB, Witte MD, Blum G, Bogyo M. Design of cell-permeable, fluorescent activity-based probes for the lysosomal cysteine protease asparaginyl endopeptidase (AEP)/legumain. *Bioorg Med Chem Lett*. 2007;17(3):649-653.
21. Kato D, Boatright KM, Berger AB, et al. Activity-based probes that target diverse cysteine protease families. *Nat Chem Biol*. 2005;1(1):33-38.
22. Yuan F, Verhelst SH, Blum G, Coussens LM, Bogyo M. A selective activity-based probe for the papain family cysteine protease dipeptidyl peptidase I/cathepsin C. *J Am Chem Soc*. 2006;128(17):5616-5617.
23. de Boer E, Moore LS, Warram JM, et al. On the horizon: optical imaging for cutaneous squamous cell carcinoma. *Head Neck*. 2016;38(Suppl 1):E2204-13.
24. Mitsunaga M, Kosaka N, Choyke PL, et al. Fluorescence endoscopic detection of murine colitis-associated colon cancer by topically applied enzymatically rapid-activatable probe. *Gut*. 2013;62(8):1179-1186.
25. Verdoes M, Edgington LE, Scheeren FA, et al. A nonpeptidic cathepsin S activity-based probe for noninvasive optical imaging of tumor-associated macrophages. *Chem Biol*. 2012; 19(5):619-628.
26. Brancaleon L, Durkin AJ, Tu JH, Menaker G, Fallon JD, Kollias N. In vivo fluorescence spectroscopy of nonmelanoma skin cancer. *Photochem Photobiol*. 2001;73(2):178-183.
27. Kamrava SK, Behtaj M, Ghavami Y, et al. Evaluation of diagnostic values of photodynamic diagnosis in identifying the dermal and mucosal squamous cell carcinoma. *Photodiagnosis Photodyn Ther*. 2012;9(4):293-298.
28. Jeon SY, Kim KH, Song KH. Efficacy of photodynamic diagnosis-guided Mohs micrographic surgery in primary squamous cell carcinoma. *Dermatol Surg*. 2013;39(12):1774-1783.
29. Heath CH, Deep NL, Beck LN, et al. Use of panitumumab-IRDye800 to image cutaneous head and neck cancer in mice. *Otolaryngol Head Neck Surg*. 2013;148(6):982-990.
30. Urano Y, Sakabe M, Kosaka N, et al. Rapid cancer detection by topically spraying a γ-glutamyltranspeptidase—activated fluorescent probe. *Sci Transl Med*. 2011;3:110ra119.
31. Segal E, Prestwood TR, van der Linden WA, et al. Detection of intestinal cancer by local, topical application of a quenched fluorescence probe for cysteine cathepsins. *Chem Biol*. 2015; 22(1):148-158.

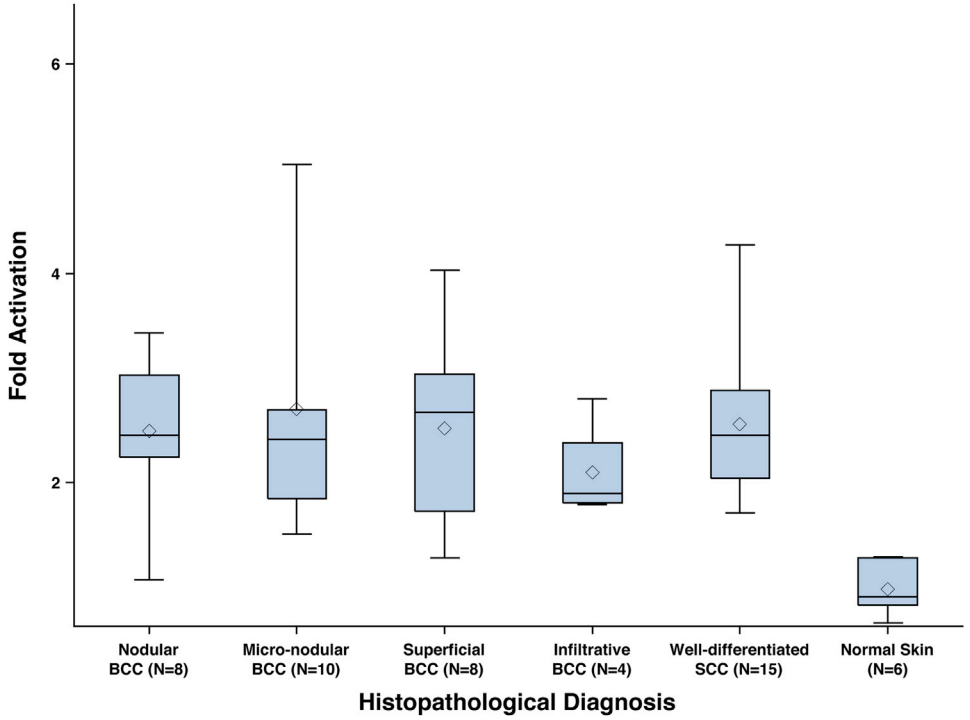

eFig 1. Probe fold-activation by histopathological diagnosis. GB119/cathepsin-dependent Cy5-fluorescent signal was normalized to imaging area and fold-activation was calculated by dividing the signal from activated probe (5 minutes after treatment) by signal from nontreated (0 minutes) samples. Fold-activation is displayed by histopathological diagnosis using box plots. The bottom and top of each box, respectively, represent the 25th and 75th percentiles, and the lines outside the box extend to the minimum and maximum value. The horizontal line inside the box and the diamond represent the sample median and mean, respectively. Statistical analysis was performed only on data from subtypes that were derived from 4 or more samples. In a 1-way analysis of variance comparing means of log-transformed fold-activations among histologic diagnoses with Tukey adjustment for multiple comparisons, activation was significantly lower in normal-appearing skin compared with all histologic subtypes (adjusted P values $\leq .01$), whereas there were no statistically significant differences among any histologic diagnostic groups. *BCC*, Basal cell carcinoma; *SCC*, squamous cell carcinoma.

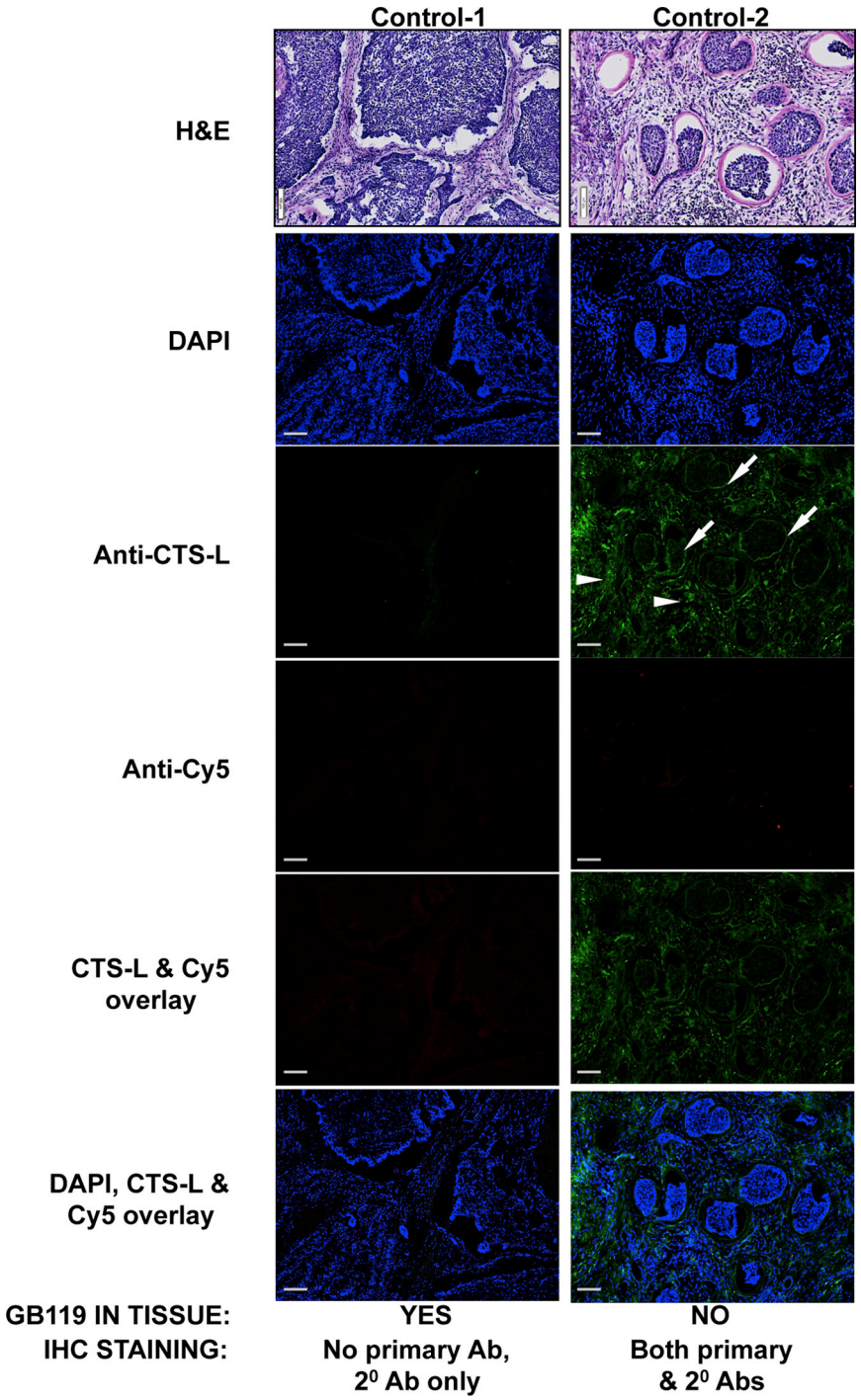

eFig 2. Immunohistochemistry (*IHC*) controls for detection of probe activation and cathepsin (*CTS*)-L (*green*) expression in basal cell carcinoma (BCC)-containing human skin tissue. Breadloaf sections of the human skin tissue treated with GB119 (*Control-1* column) or dimethylsulfoxide as a solvent alone (*Control-2* column) and used to assess the specificity of anti-Cy5 and anti-CTS-L antibodies to their target molecules. Control-1 column represents IHC staining of the BCC slides adjacent to hematoxylin-eosin (*H&E*) slide without primary antibodies. No signal for either CTS-L or activated GB119 was detectable. Inclusion of the primary antibody drastically increases signal (eFig 6, *B*, and Fig 2, *B*). Control-2 column represents IHC staining of the skin tissue not pretreated with GB119, ie, it was Cy5-free, but both primary anti-Cy5 and anti-CTS-L antibody and secondary antibodies were included. CTS-L is expressed as a zymogen and expression may not correlate with its activity. Increased levels of CTS-L expression were detected at the edge of BCC "nests" (*white arrows*) and interface (*white arrowheads*) (Control-2), because of inclusion of the primary antibody against CTS-L. However, anti-Cy5 antibody was highly specific to its target molecule and never stained BCC nests in the GB119-free samples, which were pretreated only with solvent (Control-2). H&E and IHC scale bars = 100 μm. Nuclei, 4′,6-diamidino-2-phenylindole (*DAPI*) (*blue*); Cy5, as a part of the probe (*red*). One of 10 BCC (control-1) and 1 of 4 (Control-2) representative samples is shown.

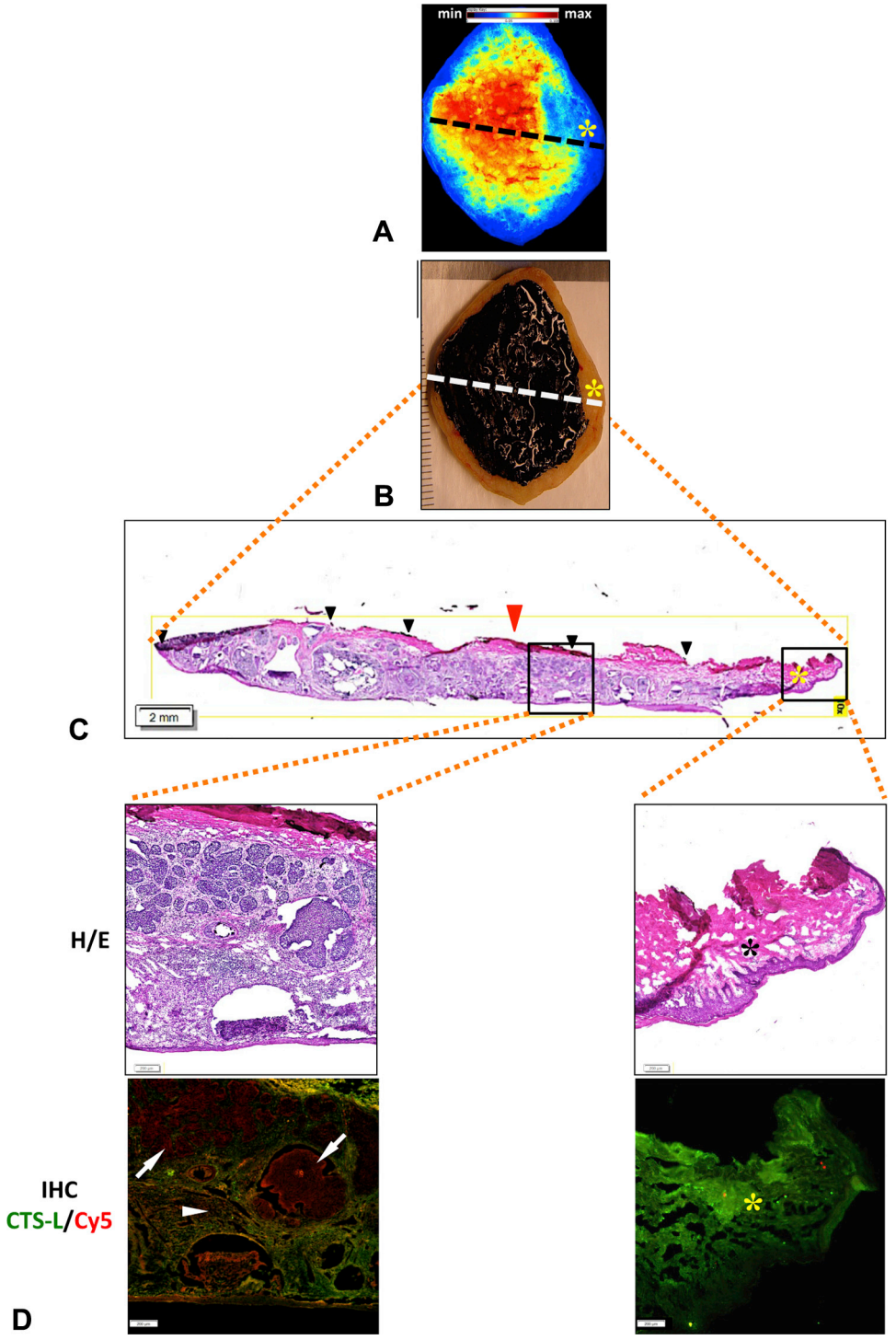

eFig 3. Assessment of depth of penetration and activation of GB119 in human basal cell carcinoma (BCC). **A**, Cy5-fluorescent images of dermal side of the human BCC skin specimen after 5-minute topical application of GB119. *Dotted line*, virtual line of sectioning. **B**, Color photograph of dermal side of the human BCC skin specimen after inking of fluorescent regions (hot spot) in **A**. **C**, Hematoxylin-eosin (*H&E*) histology image of breadloaf section corresponding to the dotted line in **A** and **B**. *Black arrowheads*, presence of pathology ink demarking fluorescence in fresh sample, **A**. *Red arrowhead*, surface of application of GB119 (dermal side) and direction of its penetration into the samples. **D**, Coregistration of activated probe, cathepsin (*CTS*)-L and cancerous (*left*) or normal (*right*) tissues. *Black arrowheads*, location of ink from **B** locating activation of applied GB119. Overlays show that CTS-L, probe

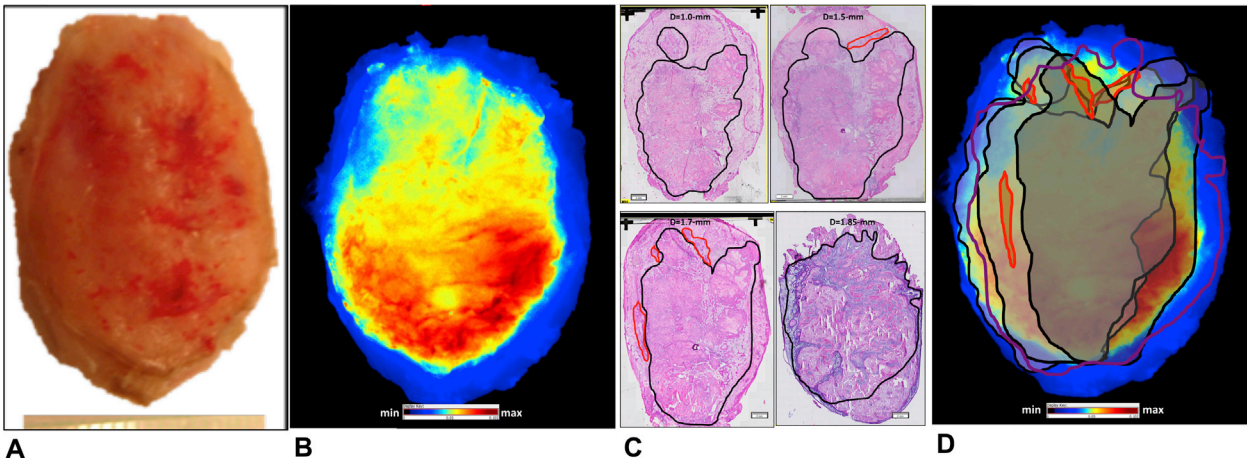

eFig 4. Correlation of pathology throughout the squamous cell carcinoma (SCC) specimen with 2-dimensional (2D) fluorescence imaging. **A**, Color photograph of dermal side of skin sample with a ruler. **B**, Cy5-fluorescence of skin sample pretreated with GB119, topically applied to skin specimens containing cancer. After 5 minutes the sample was imaged using the Maestro imaging device (PerkinElmer, Waltham, MA) and then frozen en face sections were collected. **C**, En face section histology at different depths. After hematoxylin-eosin staining, pathologists determined location of the cancer within the section and outlined the cancer with black contour lines. Section depths 1.0, 1.5, 1.7, and 1.85 mm. Scale bars = 2 mm. **D**, Overlay of contours on the 2D fluorescence image of the skin sample. The contours were overlaid on the 2D fluorescence image of the skin sample to identify the location of the cancer relative to the fluorescent signal. *Black contours*, cancer perimeter at different depth. *Purple contour*, SCC area at depth = 1.85 mm. *Red contours*, zones of tissue inflammation. One of 3 SCC representative samples is shown.

activation, and cancer colocalize throughout the samples, which is 2.5 mm in thickness (*left*). *White arrows*, BCC "nests"; *white arrowhead*, BCC nest interface. *Yellow/orange/brown*, coregistration, if any, of CTS-L and Cy5. Right, regions of normal-appearing skin within the sample do not activate the probe. Conclusion: Thickness of this particular sample was 2.4 to 2.5 mm. immunohistochemistry analysis shows a presence of yellow/orange/brown in **D** everywhere in the sample indicating presence of activated GB119 all the way thought the sample, except in normal tissue.

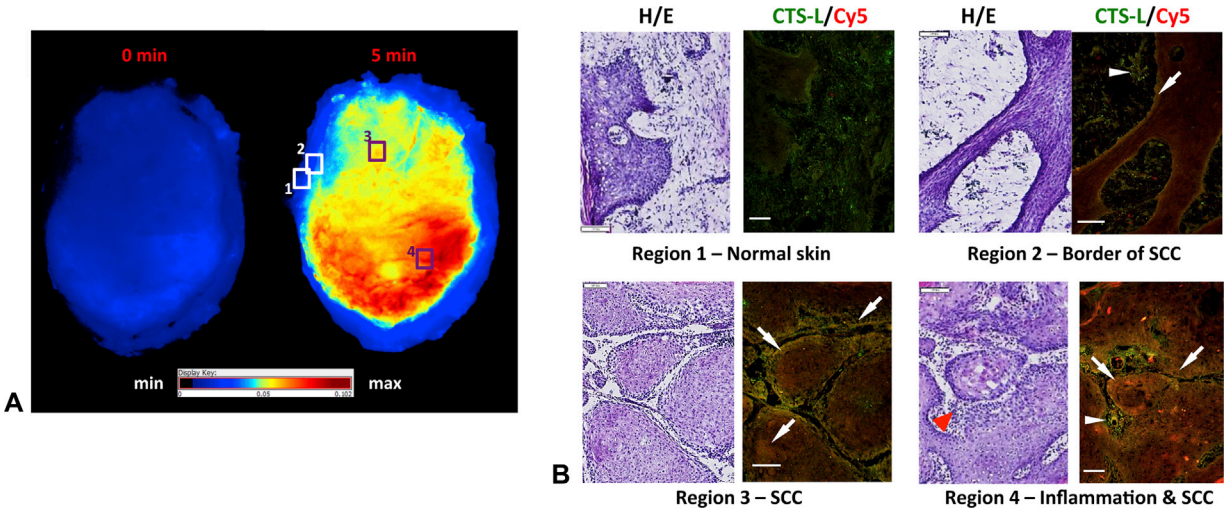

eFig 5. Microscopic analysis of regions representing different locations within the sections of squamous cell carcinoma (*SCC*) sample. Analysis of SCC specimen in eFig 3 was used to identify regions of fluorescence for further study. **A**, Cy5-fluorescence of SCC skin specimen pretreated with GB119. Nonfluorescent region (rectangle 1), region bordering fluorescence and nonfluorescent areas (rectangle 2), and areas only within the fluorescent regions (rectangles 3 and 4) were identified for further study. **B**, Co-expression of cathepsin (*CTS*)-L and Cy5 in immunohistochemistry (IHC) image overlays at different locations of sample. Specimen was subjected to frozen en face sectioning followed by hematoxylin-eosin (*H&E*) and IHC for activated GB119 and CTS-L in adjacent sections. *White arrows*, SCC "nests"; *white arrowheads*, SCC nest interface. *Orange/brown* represents coregistration of CTS-L and Cy5. *Red arrowhead*, zone of accumulation of inflammatory cells. All scale bars = 100 μm. One of 3 SCC representative samples is shown.

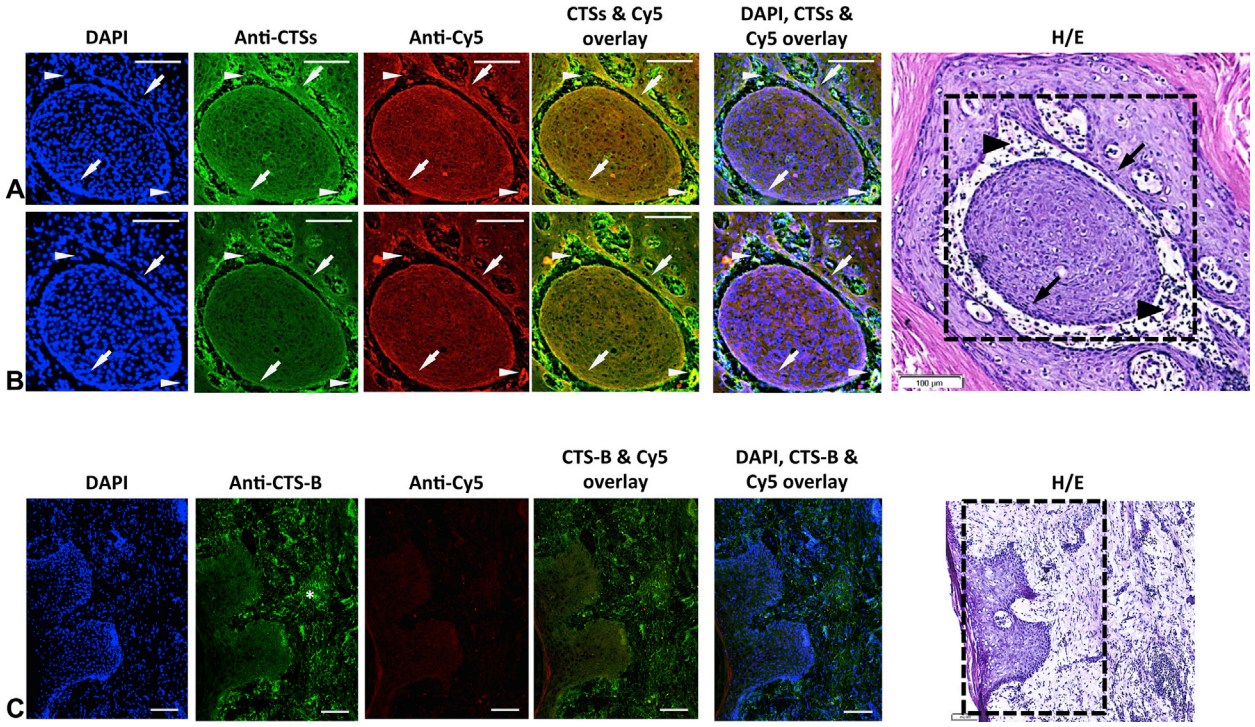

eFig 6. Correlation of probe activation to cancer and cathepsin (*CTS*)-B expression in squamous cell carcinoma (SCC)-containing human skin tissue. En face consecutive sections were used to assess the correlation of probe activation to cancer location and both CTS-B and −CTS-L (*green*) expression. Anti-CTS-B and anti-CTS-L antibody demonstrates higher expression of CTS-B (**A**) and CTS-L (**B**) in cancerous tissue (the same location in the sample, see hematoxylin-eosin [*H&E*] histology at very right) as compared with normal-appearing skin tissue (**C**). Because CTS-B and CTS-L are expressed as a zymogens and expression may not correlate with activity, we also visualized active probe by staining for activated GB119, column 3 (anti-Cy5). Overlays clearly indicate little to no probe activation in normal tissue (**C**), but high activation in cancerous tissues (**A** and **B**). Normal-appearing skin tissue expresses CTS-B (*white asterisk*) but had little staining for activated GB119. Only cancer tissue shows strong expression of CTS-B and CTS-L and strong staining for unquenched/activated probe with good coregistration (*brownish color*). *Arrows*, edges of SCC "nest"; *arrowheads*, nest interface. H/E and immunohistochemistry scale bars = 100 μm. Nuclei, 4′,6-diamidino-2-phenylindole (*DAPI*) (*blue*); Cy5 as a part of the unquenched/activated probe (*false red*). Two of 10 SCC representative samples are shown. Staining for CTS-B at the normal tissue (**C**) represents the same area as in Fig 4, *B*, region 1.

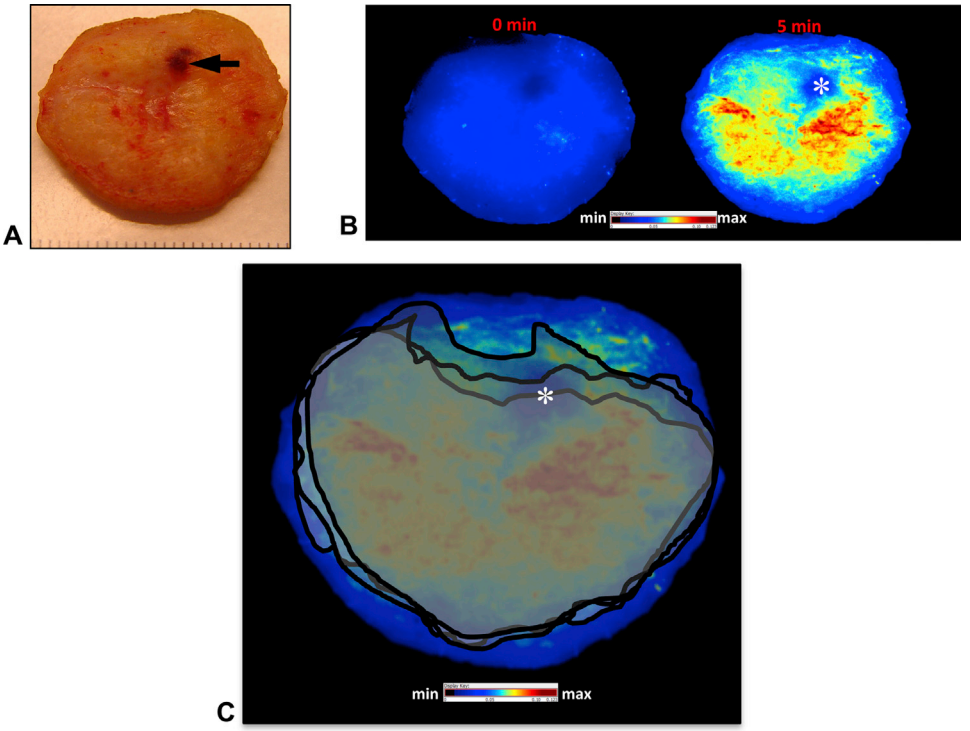

eFig 7. Effect of blood clots on the 2-dimensional (2D) fluorescence imaging. This basal cell carcinoma (BCC) skin specimen was treated with GB119, imaged, frozen, and kept at −80°C according to our protocol before histologic analysis. **A**, Color photographs of dermal side of the human BCC skin specimens before the probe application. *Black arrow*, preformed dense blood clot. Ruler bars = 1 mm. **B**, Images of Cy5-fluorescence on dermal side of the samples before (0 minutes) and after (5 minutes) topical application of the probe (Maestro imaging system; PerkinElmer, Waltham, MA). *White asterisk*, positioning of preformed dense blood clot. Note the quenching of signal that occurs in the location of the clot. **C**, Contours of BCC lesion from 3 en face pathology sections at depths of 1.0, 1.5, and 1.7 mm overlaid on to the 2D-fluorescence image (Fig 3). One of 6 BCC representative samples is shown.

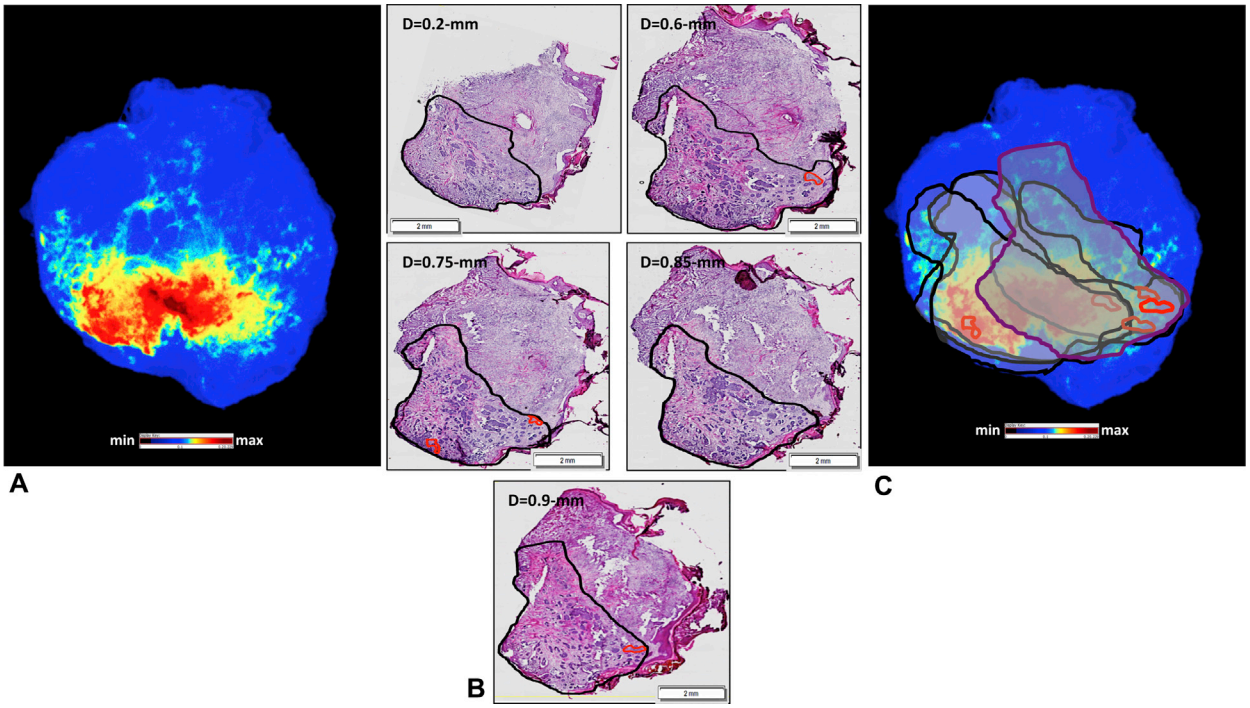

eFig 8. Correlation of pathology throughout the basal cell carcinoma (BCC) specimen with 2-dimensional (2D) fluorescence imaging. Additional example. **A**, Cy5-fluorescence of skin sample pretreated with GB119, topically applied to the dermal side of skin specimens containing cancer. After 5 minutes the sample was imaged using the Maestro imaging device (PerkinElmer, Waltham, MA) and then frozen en face sections were collected. These sections were derived from the same tissue used to derive Fig 3. **B**, En face section histology at different depths. After hematoxylin-eosin staining pathologists determined location of the cancer within the section and outlined the cancer with black contour lines. Section depths 0.2, 0.6, 0.75, 0.85, and 0.9 mm. Scale bars = 2 mm. **C**, Overlay of contours on the 2D fluorescence image of the skin sample. The contours were overlaid on the 2D fluorescence image of the skin sample to identify the location of the cancer relative to the fluorescent signal. *Black contours*, cancer perimeter at different depth. *Purple contour*, BCC area at depth = 0.90 mm. *Red contours*, zones of tissue inflammation.

eTable I. Debulked human skin specimen tumor type and tissue depth

Specimen no.	Tumor type	Tissue depth, mm*	Fold-activation of GB119†
1	BCC; N, MN	3.1-4.9	6.13
2	BCC; N	1.5-5.1	2.18
3	BCC; MN	3.1-4.3	2.70
4	BCC; I	3.1-3.9	1.97
5	SCC; MD, S	3.6-4.1	2.45
6	SCC; WD	1.9-2.2	2.63
7	BCC; MN, S	1.5-2.1	3.32
8	BCC; MN	0.9-1.3	2.52
9	BCC; I	1.1-1.8	2.80
10	BCC; S	2.1-2.8	2.59
11	BCC; MN	1.1-3.9	1.84
12	BCC; S	1.3-1.8	1.99
13	SCC; WD	0.5-0.8	4.16
14	BCC; MN	0.5-0.8	5.04
15	BCC; MN	1.1-1.8	1.51
16	SCC; WD	0.7-0.8	2.11
17	SCC; WD	0.9-1.9	2.06
18	BCC; N, MN	1.1-1.6	2.62
19	BCC; N	1.1-2.0	2.55
20	SCC; WD	0.5-1.0	2.45
21	BCC; S	0.3-0.5	4.03
22	SCC; WD	1.5-2.5	2.56
23	SCC; WD	0.7-2.5	2.88
24	SCC; WD	1.5-3.9	2.32
25	BCC; MN	2.2-5.5	4.40
26	BCC; MN	0.7-1.1	2.30
27	SCC; WD	0.5-1.2	2.65
28	SCC; MD	1.7-4.5	2.07
29	SCC; WD	0.5-0.6	1.71
30	BCC; S	0.5-1.2	1.46
31	BCC; I	1.9-2.7	1.82
32	SCC; MD	0.5-1.5	1.96
33	SCC; MD	1.3-1.8	2.85
34	BCC; S, I	0.5-1.3	2.01
35	BCC; MN	1.1-2.0	1.85
36	SCC; WD	0.4-0.5	2.91
37	BCC; N, MN	1.4-2.5	2.41
38	BCC; MN	0.5-1.8	2.62
39	BCC; N	2.1-3.8	2.36
40	BCC; S	3.0-4.2	2.75
41	SCC; WD	0.9-1.1	4.27
42	BCC; MN	0.4-0.5	2.30
43	BCC; N	0.5-1.1	2.30
44	BCC; N	0.5-0.9	1.07
45	BCC; I	0.8-2.5	1.79
46	BCC; N	0.9-1.5	3.43
47	SCC; WD	0.5-1.2	1.79
48	BCC; S	0.3-0.5	3.07
49	BCC; S	0.5-1.0	3.00
50	SCC; WD, MD	0.5-1.5	2.38
51	BCC; N	0.5-1.0	2.62
52	SCC; WD	0.8-1.1	1.85
53	SCC; WD	1.5-4.0	2.04
54	BCC; S	0.2-0.3	1.28
55	BCC; N	1.0-1.3	3.43
56	SCC; WD, MD	1.1-3.9	1.92
57	BCC; MN, I	0.9-2.4	2.20
58	BCC; I	0.8-3.1	2.25
59	SCC; WD	0.8-3.9	2.25
60	BCC; N	1.0-2.4	2.60
61	BCC; I	0.8-3.2	2.10
62	BCC; S	0.4-3.3	1.97
63	BCC; S	0.4-2.0	1.93
64	SCC; WD	1.2-2.3	2.11

Breadloaf and en face frozen sections (histology and hematoxylin-eosin) were used for specimens 1-55 and 56-64, respectively. Samples 1-55 were used to assess both sensitivity and specificity of the method.

BCC, Basal cell carcinoma; *I*, infiltrative; *MD*, mildly differentiated; *MN*, micronodular; *N*, nodular; *S*, superficial; *SCC*, squamous cell carcinoma; *WD*, well differentiated.

*Represented as a minimum and maximum distance between dermal and epidermal edges of the skin tissue on hematoxylin-eosin histology slide for each sample.

†Represents GB119/cathepsin-dependent Cy5-fluorescent signal that was normalized to imaging area. Fold-activation was calculated by dividing the signal from activated probe (5 minutes after treatment) by signal from nontreated (0 minutes) samples.